

A Semi-empirical Approach to Simulate the Effects of Higher Harmonic Rotor Blade Control Using Prescribed Wake

Application in a Comprehensive Rotor Code and Validation with HART II Data

Berend G. van der Wall¹, Jianping Yin²

¹Institute of Flight Systems, ²Institute of Aerodynamics and Flow Technology

German Aerospace Center (DLR), Lilienthalplatz 7, 38108 Braunschweig, Germany

¹berend.vanderwall@dlr.de; ²jianping.yin@dlr.de

Abstract

To account for the effect of higher harmonic rotor blade control (HHC) on the wake geometry and hence on blade-vortex interaction (BVI) locations, free-wake methods are regularly used within comprehensive rotor simulation environments. Prescribed wake formulations are much faster than free-wake codes, but they require simplified *a priori* information of the induced velocity field within the rotor disk to compute the wake perturbations generated by them. In this paper, a semi-empirical approach to account for the effects of HHC on the prescribed wake geometry is described and validated against data from the 2nd HHC Aeroacoustic Rotor Test (HART II). This covers the computation of the global induced velocity perturbations due to HHC from the blade loading time histories, the computation of the wake geometry perturbations due to these (both are performed within DLR's high resolution comprehensive rotor code S4), and finally the noise radiation using DLR's acoustic code APSIM. The results have first been presented at the American Helicopter Society 65th Annual Forum, Grapevine, Texas, May 27-29, 2009.

Keywords

Helicopter Rotor Acoustics; HART II; HHC; Prescribed Wake

Introduction

In 2001, the second Higher Harmonic Control (HHC) Aeroacoustic Rotor Test (HART II) was jointly performed by US Army AFDD, NASA Langley, DLR, ONERA and DNW, [18], with the purpose of the generation of a comprehensive data base of a 40% Mach-scaled Bo105 hingeless model rotor in descent flight condition where strong blade-vortex interaction (BVI) takes place. Measurements of rotor loads, blade leading edge and – at one radial station – chordwise pressure distribution, and blade deformation by means of stereo pattern recognition (SPR) [15] were performed. Additional measurements covered the acoustic radia-

tion and wind tunnel data. The emphasis was placed on measurements of wake vortex trajectories and velocity fields of individual tip vortices throughout the entire rotor disk. For this purpose, stereo particle image velocimetry (3C-PIV) was applied to obtain all three velocity components within the measurement plane. A large amount of work was spent on analysis of the PIV data to extract vortex positions in space and vortex parameters like core radius, swirl velocity profiles, and dependency of these on vortex age [3], [19]. These data were used for code validation activities within the HART II team [11], [12], [14] and [20]. In 2005, an international workshop was established where part of the data were made available to the international community for purposes of code validation [16]. Since then, regular workshop meetings took place at both the AHS Annual Forum and the European Rotorcraft Forum. In most cases, these code validations utilized a loose (or soft) coupling approach of some sort of computational structural mechanics code (CSD) with a computational fluid dynamics code (CFD), mainly based on the solution of the Navier-Stokes equations. Numerous publications have evolved from this workshop activity, like refs. [4], [6] and [7].

While the CFD/CSD approach in general has the potential of highest fidelity results the most crucial point of the solution quality is to conserve the tip vortices for the duration of at least two rotor revolutions. Various attempts have been made to address this issue properly, amongst which a tremendous increase of grid cells beyond 100 million and higher order schemes [12], chimera grids for the tip vortices [4], a mixture of Navier-Stokes and Euler solutions [7], as well as hybrid approaches like coupling of CFD for the air loads with vortex lattice models for the wake [6] were shown. Lower order modeling included the ap-

plication of free-wake codes [14], and even prescribed wake with additional wake deflections due to harmonic rotor disk loading [20], where the underlying physics and modeling were published in ref. [21]. Compared to the CSD/CFD approaches, the usage of comprehensive codes with engineering reduced-order models for the structural dynamics, semi-empirical modeling of unsteady aerodynamics and vortex lattice modeling of the wake reduces the computational expense by several orders of magnitude. Compared to a free-wake approach, a prescribed wake again can reduce the computational effort by as much as one to two orders of magnitude. However, comprehensive codes require a proper representation of all the important physical phenomena that contribute to the desired solution. For the BVI noise radiation issue, these are:

- Blade elastic motion in flap (first three modes), lead-lag (first two modes) and torsion (first mode) in the frequency range of up to about 8/rev
- Unsteady aerodynamics up to very high frequencies (BVI loading, up to about 160/rev)
- Wake geometry and induced velocities

While the blade motion due to its relatively low frequency content requires only a moderate resolution in time (i.e. azimuth; $\Delta\Psi \approx 10^\circ$) and space (i.e. radius; about 10 blade elements), the air loads needed for computation of the acoustic radiation may require both a high resolution in time ($\Delta\Psi \leq 1^\circ$) and space (≥ 20 blade elements). The wake geometry is essential for the BVI locations within the rotor disk and the tip vortex' circulation strength and swirl velocity profile is crucial for the induced velocities at the blade as input for the aerodynamic response. The high frequency air loads response in return is the source of the noise radiation computation. Thus, any piece of this computational chain must be of appropriate accuracy in order to compute BVI noise to a sufficient degree of accuracy. The purpose of this paper is to demonstrate that even with prescribed wake codes the phenomena of active control can properly be addressed up to the computation of BVI noise radiation. A key figure is the need to deform the wake geometry that is associated with higher harmonic loading distribution within the rotor disk.

Computational Chain

The working horse for isolated rotor simulation with high resolution at DLR is the S4 code (4th generation simulation code) [22]. Its first module, the structural

mechanics part, consists of a pre-processor based on finite element analysis that provides natural modes and frequencies of the rotor blades in flap, lead-lag and torsion. During the rotor simulation, the dynamic response problem is solved by numerical integration based on a Runge-Kutta 4th order scheme with constant time stepping of 2° azimuth. The radial discretization is usually 20 blade elements with constant annulus area, thus giving a concentration of elements and associated high spatial resolution towards the blade tip where the largest aerodynamic forces act.

The second module is the semi-empirical unsteady aerodynamics routine, which describes the steady aerodynamic coefficients via mathematical formulas as a function of the Mach number components along the chordline direction, normal to it and the one in radial direction which generates a yaw angle. Its origins is from the formulation of Leiss [10] with multiple modifications and enhancements incorporated during the march of time. This aero model accounts for compressibility effects, stall and the effects of yaw. The unsteady model consists of two parts. Firstly, the geometric angle of attack time history as computed by the time history of blade motion and the Mach components is transformed into an effective angle of attack time history by means of the indicial function approach in conjunction with the arbitrary motion theory [22]. In the incompressible case, this reduces Theodorsen's lift transfer function [17]. Secondly, the effective stall angle is similarly computed, but with different time lag, which allows for computation of dynamic stall to a first order accuracy. However, for the operational condition of this paper, no stall computation is needed.

BVI related air loads are handled separately. Their input is the high frequency induced velocity part of the wake and the lift transfer function is different from that of the airfoil motion, since physically it is the problem of a gust with the vortex-induced velocity disturbance traveling over the chord of the section of interest. Thus, in the incompressible case, this reduces to Küssner's lift transfer function [8]. The main difference to the airfoil motion response is that at very high frequencies the gust transfer function approaches zero while the lift transfer function due to airfoil motion approaches 0.5. This leads to a much larger dynamic response reduction in the case of a gust compared to the case of airfoil motion. However, in steady conditions both functions start from 1 and the quasi-steady behavior is very similar for both.

The third part of S4's computational chain is the prescribed wake module [21]. In its origins, it is based on Beddoes' prescribed wake, ref. [1] (which is also described in ref. [9], p. 457-458), corrected for the mean part of the underlying momentum theory induced velocity model, which is needed for computation of vortex trajectories in space and time. In S4, the entire tip vortex spiral is used, in contrast to Beddoes' further simplification replacing every vortex spiral by two straight vortices. The radial position of the tip vortex is computed based on the radial loading distribution on the blade, and multiple vortices of even different sense of rotation can be included dependent on the blade loading. For example, in high speed the second quadrant of the rotor disk often experiences a download instead of lift at the blade tip, thus emitting a pair of counter-rotating tip vortices. In addition, higher harmonic control (HHC) can generate download at the blade tip area over a range of azimuth, which as well generates such a vortex pair.

Beddoes wake geometry only depends on the mean thrust and the global operating conditions and thus any effect of harmonic rotor loading on induced inflow and consequently on vortex trajectories is neglected. Therefore, it is insensitive to HHC, harmonic loading due to flight condition, or any other active control. The method described in this article pays more attention to the harmonic rotor loading which generates an associated harmonic inflow (based on momentum theory approach) that in turn modifies the vortex trajectories. In this way the vortex trajectories are sensitive to amplitude and phase of any sort of active control, and as well they are sensitive to any harmonic loading of the rotor such as in high-speed flight. This is the key feature that makes prescribed wakes applicable to BVI noise radiation computations [20], [21].

Based on S4 airloads as input, the sound propagation into the far field is calculated with APSIM. The methodology of APSIM is based on both permeable and non-permeable Ffowcs Williams-Hawkins (FW-H) formulation [9] as well as Kirchhoff formulations [2]. Only linear sound propagation is taken into account when the sound propagates away from the noise source surface. In this paper, acoustic results based on non-permeable FW-H surfaces method are applied to appropriately account for the monopole and dipole sources. The quadrupole noise contributions are not considered and assumed to be negligible for the flight conditions used in the paper. The calculations performed in the time domain, deliver a pressure time

history at any observer location. This sound pressure time history is transformed into a Fourier series to obtain the acoustic spectrum. A more detailed description of the implemented approaches and of the APSIM code can be found in ref. [23].

Modelling of the Wake

Any prescribed wake model requires an underlying model for the induced inflow field λ_i as a function of x and y (λ_i = induced velocity (pos. down), made non-dimensional by the rotor blade tip speed ΩR (wherein Ω is the rotor rotational frequency and R is the rotor radius); x , y , z = rotor hub coordinates; x pos. downstream, y pos. starboard, z pos. up). Thus, the vertical displacement of the tip vortices, z , can be computed by means of integration along its path downstream from the point of creation and requires the induced velocities along this path. For this purpose, global induced inflow models of lower order are the best suitable for ease of integration. In general, these can be formulated with slope factors k_x and k_y like

$$\frac{\lambda_i}{\lambda_{i0}} = k_0 + k_x \frac{x}{R} + k_y \frac{y}{R} + k_{y3} \left| \frac{y}{R} \right|^3$$

Generally, $k_0 = 1$ and $k_y = k_{y3} = 0$ are used. The mean induced inflow λ_{i0} is computed iteratively by means of momentum theory (see ref. [9], p. 66-67) while the lateral and longitudinal gradients require deeper knowledge of the wake structure. A list of various sources from 1945 until 1981 is given in ref. [9], p. 118. To better account for roll-up of the wake at the sides of the disk, Beddoes [1] added the cubic part in y wherein $k_{y3} = -k_x$. However, due to the absolute value of $|y/R|^3$ taken, this violates the momentum theory since the mean part of the inflow is not unity any more. Thus, as outlined in ref. [21], a correction to the mean part must be applied such that

$$k_0 = 1 - \frac{8k_{y3}}{15\pi}$$

Rotor Operating Condition

The mean operating condition investigated here is a 6° descent flight at an advance ratio of $\mu = 0.151$ and a thrust coefficient of $C_T = 0.0044$. The rotor is a Mach scaled 40% model of the Bo105 main rotor with $N = 4$ blades, $R = 2\text{m}$ radius and a solidity of $\sigma = Nc/(\pi R) = 0.077$ (the full-scale Bo105 has $\sigma = 0.07$ and the model chord c is slightly increased relative to the full-scale rotor to account for Reynolds number effects). The

shaft angle is nose-up with $\alpha = 5.3^\circ$ in the 6m x 8m open jet test section of the DNW, which – after application of wind tunnel corrections – reduces to effectively about 4.3° relative to the wind. In this situation, severe BVI noise is radiated from interactions in the first and fourth quadrant of the disk. Thus, the blade tip vortices must pass the rotor disk in these areas.

Induced Inflow Distribution and Vortex Trajectory

Vortex positions have been measured in HART II at $y/R = \pm 0.7$ from the point of creation downstream the disk and can be compared with the positions computed from the prescribed wake. Furthermore, the induced velocities at these positions can be extracted from the measurements and can as well be compared with the induced velocity distributions of the various low-order models. A list of results for the longitudinal and lateral inflow gradients obtained with the formulas of various authors, see ref. [9], p. 118, is given in Table 1.

TABLE 1 ESTIMATED VALUES OF FIRST HARMONIC INFLOW

$$(C_T = 0.0044, \mu = 0.151, \alpha_{\text{eff}} = 4.3^\circ, \lambda_0 = 0.0146)$$

Author	k_x	k_y	k_{y3}
Coleman et. al.	0.978		
Drees	1.250	-0.302	
Payne	1.300		
White & Blake	1.414		
Pitt & Peters	2.005		
Howlett	1.000		
Beddoes	1.549		-1.549
Mangler	2.880		
HART II	3.564		

Additionally, a higher order global inflow model is given by Mangler. Therein, the steady part as well as the first harmonic part has radial shape functions and a magnification dependent on the rotor disk angle of attack, see ref. [13]. Although the distribution is highly nonlinear, a linear slope can be approximated and identified by means of a regression. Except for the Mangler model, the longitudinal slope is insensitive to the lateral position within the disk. For the lateral position of $y/R = 0.7$ (advancing side) these gradients are summarized in Table 1 and the induced velocity distributions of these models are shown in Fig. 1. Data identified by velocity measurements of HART II are given as well, but probably biased to some degree due to the presence of the tip vortices. Most of the models are close to each other, have a common point at $x/R = 0$, but have different gradients. Drees' model also has a lateral gradient which offsets the velocity distribution at this lateral position to lower values, which physi-

cally means that on the advancing side more upwash relative to the retreating side is predicted in his model. Beddoes' uncorrected model shows even more upwash (on both sides of the disk) while the correction for the mean downwash makes his model closer to Drees' curve.

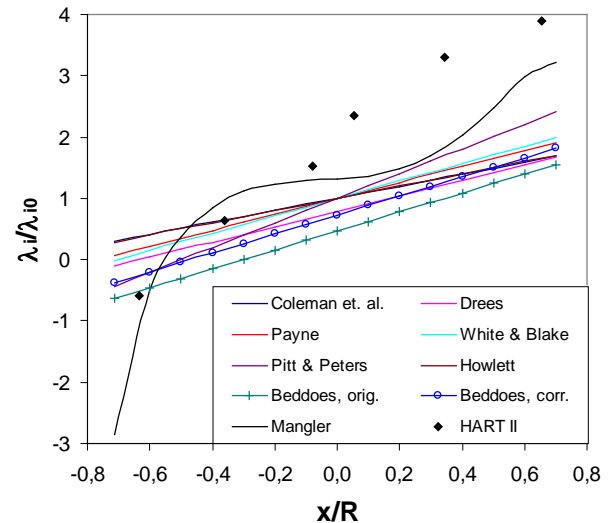
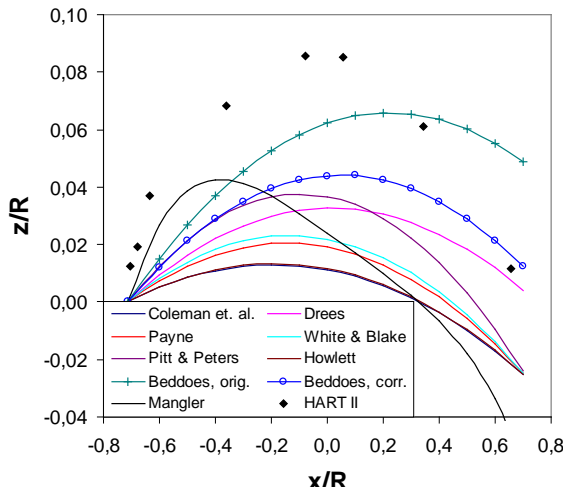


FIG. 1 INDUCED INFLOW DISTRIBUTION AT $y/R = 0.7$

In contrast to these low-order models, the higher-order model of Mangler (only the steady and first harmonic part taken into account) has already given a highly non-uniform inflow distribution with a much larger longitudinal gradient, see Table 1. In addition, the HART II data do not show the non-linearity of Mangler's model, rather a more linear increase of induced flow, but with about twice of the gradients suggested by all the models.

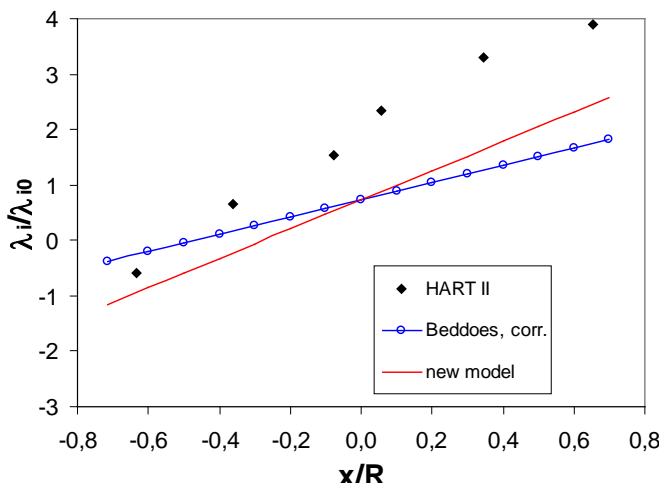
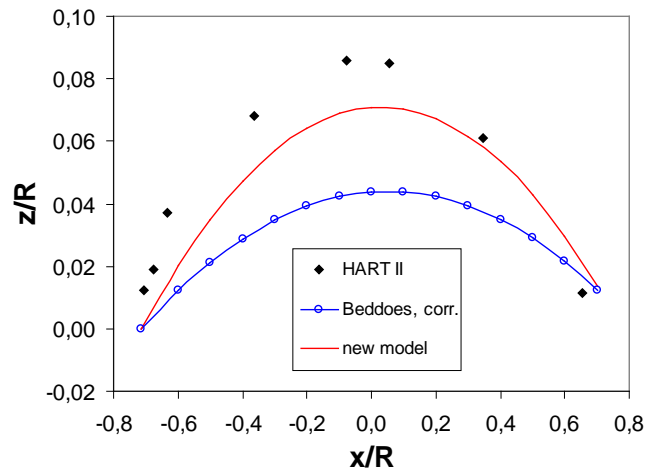
The integration of all vertical velocities downstream of the point of tip vortex creation generates the tip vortex trajectory, i.e. its flight path through the rotor disk. To simplify the computation in the case of Mangler's velocity distribution, first of all, a regression with a third order polynomial is made, which is used for computation of the trajectory. For all other models the data of Table 1 are used and the HART II data are taken from the experiment, corrected for the mean blade tip vertical position. The result is shown in Fig. 2. Those models that only differ in the gradient of induced flow also differ only in the amount of vertical deflection of the trajectory, but it begins and ends in a common point. Drees' and Beddoes' models have more upwash on the advancing side, thus their trajectories end at higher positions. Correcting Beddoes' model with respect to the mean part lowers the trajectory close to Drees', but the larger gradient of Beddoes' model results in larger vertical deflections.

FIG. 2 TIP VORTEX TRAJECTORY AT $y/R = 0.7$

The Mangler model initially shows a steep rise of the vortex, but then quickly turns this trend to the opposite due to its steep increase of downwash as seen in Fig. 1. Except for the first part of Mangler's model, none of the models is able to predict the tip vortex trajectory close to the measured positions, although the corrected Beddoes model nicely matches where the vortex comes close to the disk to generate BVI.

Induced Inflow Model Enhancements

Therefore, it is suggested that 1.7 times of the amount of the longitudinal induced flow gradient of Beddoes' model (i.e., $k_x = 2.633$) is used in order to better represent the induced velocity slope of the experiment (while the old value for the lateral gradient, i.e. k_{y3} , remains unchanged) and obtain deflections of the tip vortex trajectory as measured. The results are shown in Fig. 3 and Fig. 4 and the agreement with experimental data is much better than that with the conventional models.

FIG. 3 INDUCED INFLOW DISTRIBUTION AT $y/R = 0.7$ FIG. 4 TIP VORTEX TRAJECTORY AT $y/R = 0.7$

In addition to this modification, the induced inflow model of the prescribed wake has an extra part based on the harmonic content of the lift distribution in the rotor disk. As described in detail in ref. [21], the harmonic part of the lift is associated with a harmonic downwash distribution following the momentum theory. The tip vortices have to pass these additional downwash distributions along their way downstream through the rotor disk and thus gaining additional vertical deflections that depend on magnitude, phase and frequency of the harmonic lift content. In this way the prescribed wake geometry becomes sensitive to any HHC related loading and as well to harmonic loading due to the flight condition, or other active control.

With or without this part, in any case the azimuthal circulation distribution of the wake tip vortices depends on the azimuthal blade loading distribution. Thus, the global induced velocities are only marginally affected by the inclusion of the HHC wake geometry module and the low frequency aerodynamics as well as the associated blade dynamics are mainly unchanged. In contrast, the BVI interaction geometry, and with it the high frequency aerodynamic content of the aerodynamic loading which is the driving parameter for noise radiation, highly depend on this HHC wake module.

An example for the additional wake deformations due to a 3/rev HHC with control for minimum noise (MN) and minimum vibration (MV) is shown in Fig. 5 (taken from ref. [21]; in this figure x, y, z are coordinates made non-dimensional by the rotor radius R). In the MN case, the vortices are deflected downwards in the right and left side of the rotor. This is because (due to the HHC phase) in the second and third quadrant additional lift is generated, causing an additional down-

wash that in turn convects the vortices down. In the center the vortices are lifted up due to a download in the front of the disk caused by HHC, which generates an upwash that convects the vortices upwards. Due to the different control phase in the MV case, the locations of HHC-related lift and download and their up- and downwash areas are at other positions.

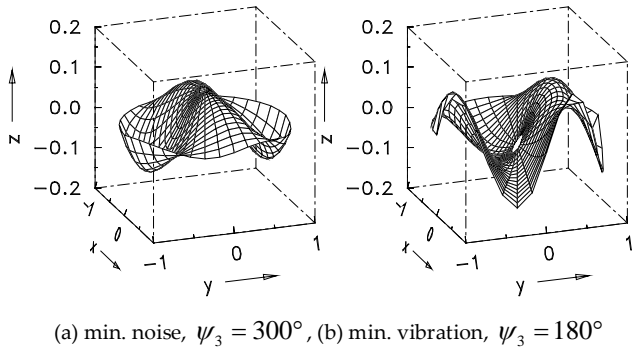


FIG. 5 NORMALIZED WAKE DEFLECTION DUE TO 3/REV HHC

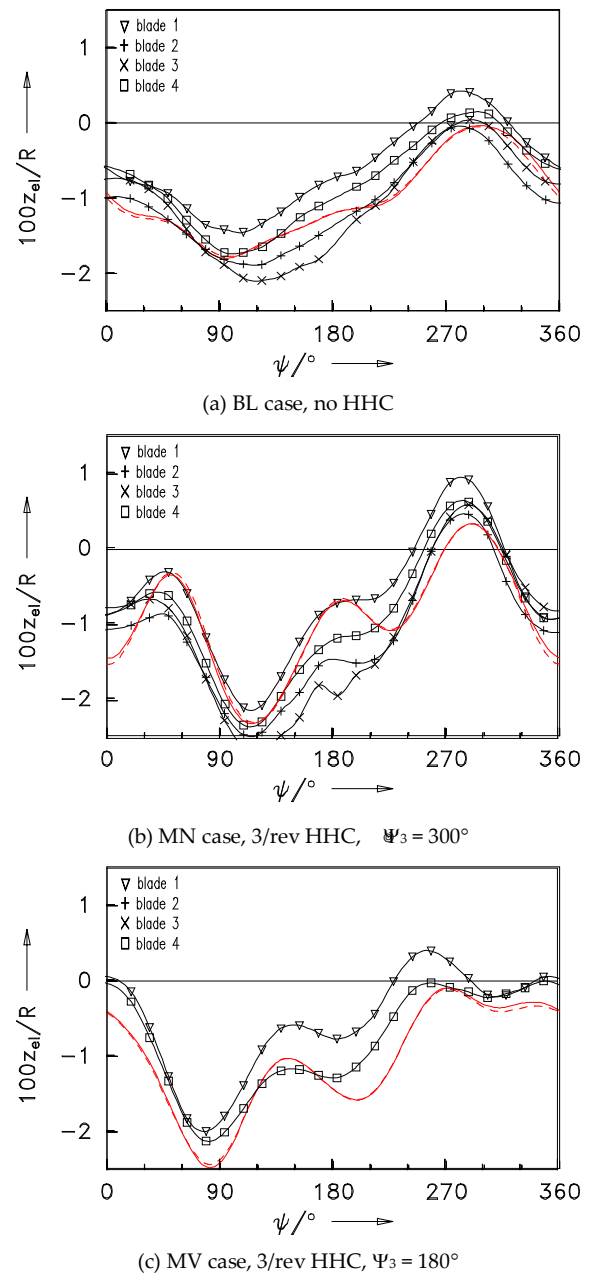
It must be recalled that these deflections are only generated by the HHC wake geometry module, while all classical prescribed wake codes do not change the wake geometry whatever the loading distribution within the rotor disk looks like. Consequently, the only change of BVI locations in all the classical prescribed wake codes is purely due to a different blade position at both the azimuth of vortex creation and the azimuth of BVI locations. The blade deflections due to HHC, however, are one order of magnitude less than the wake deflections, see refs. [16], [18], and thus by far insufficient to address the problem appropriately.

Application to the HART II Cases

The computational chain is now applied to simulate the operational conditions of 1) the HART II baseline case (BL), i.e. without HHC; 2) the minimum noise case (MN) with 3/rev HHC and a pitch amplitude of $\Psi_3 = 0.8^\circ$ with a phase of $\Psi_3 = 300^\circ$ at the blade root; and 3) the minimum vibration case (MV) with the same HHC pitch amplitude but a different phase of $\Psi_3 = 180^\circ$. The computations are based on three flap modes, two lead-lag modes and the first torsion mode and the rotor is retrimmed in any case.

For a proper computation of BVI, the blade motion must be simulated to a sufficient degree of accuracy since the blade motion a) partly influences the aerodynamic loading and with it the circulation that is fed into the wake system, b) defines the position in space where tip vortices are released into the flow and c) the blade position is important at the locations where BVI takes place since it partially defines the blade-vortex

miss-distance that is important for the BVI intensity.



Red: S4 simulation (solid: without, dash: with HHC wake module), black: HART II experiment

FIG. 6 VERTICAL BLADE TIP DEFLECTION

Simulated results for the vertical blade tip deflection are compared to HART II experimental data in Fig. 6 (a) for the BL case, in (b) for MN and in (c) for MV. The red lines are the simulation, wherein the solid line is without the HHC wake geometry module and the dashed line with this module. Since they are virtually the same, there is almost no difference with respect to blade motion. This is plausible since the blade motion is caused by the low frequency range of about 0-6/rev of the air loads and these are virtually unaffected by some tip vortex position changes.

Of most importance for correct air loads, simulation is the dynamic blade response in elastic torsion, especially for soft-in-torsion blades like those of the Bo105 with a natural frequency of about 3.6/rev, i.e. close to the HHC control frequency of 3/rev. Due to this proximity, a large magnification is to be expected. Finally the torsion adds to the local angle of attack and thus affects the lift, which in turn defines the tip vortex strength and its trajectory.

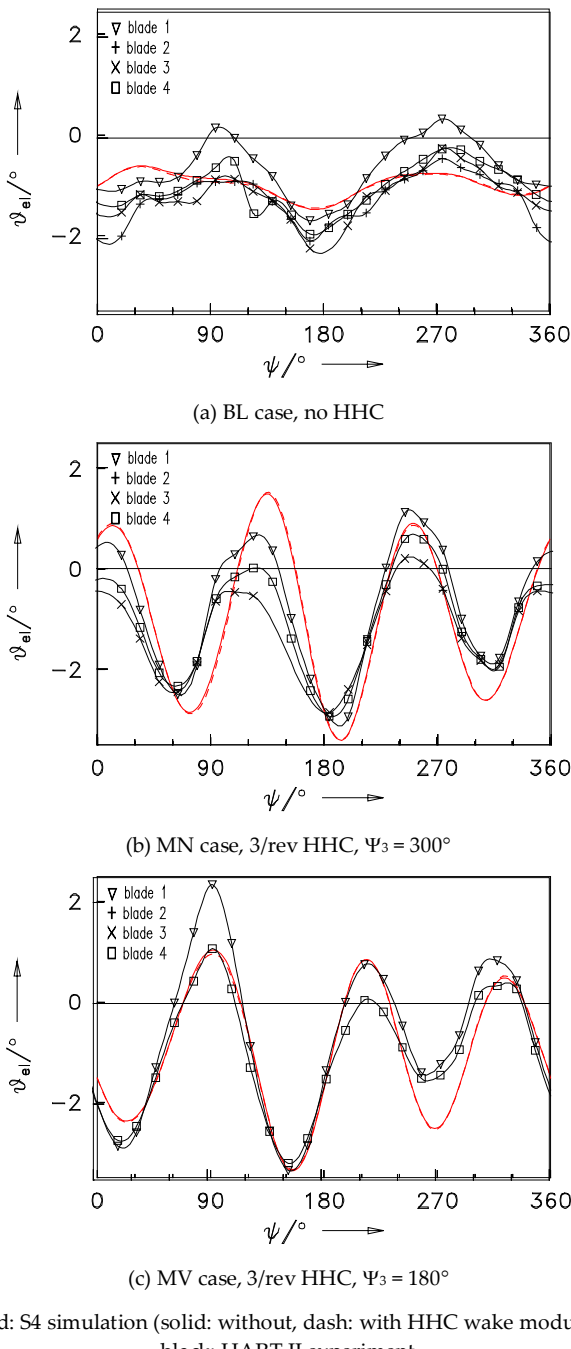


FIG. 7 BLADE TIP ELASTIC TORSION

Results of torsion are given in Fig. 7 for the same cases as in Fig. 6. As in the flap response, the difference in simulation with or without the HHC wake geometry

module is negligible. In all the three cases, the general torsion of the blade is nicely captured, i.e. the 2/rev in the BL case (a) and in the cases of HHC (b) and (c) the agreement with the experimental data is very good. It must be kept in mind that the blade root actuation of HHC has an amplitude of only 0.8° , while the tip response has amplitudes of up to 2.5° , i.e. a magnification factor of 3. It must be noted that part of the result is due to a flap-torsion coupling since the mass axis of the rotor blade has an offset relative to the elastic axis, such that any flap acceleration directly exaggerates torsion. In addition, any flap deflection causes a torsion moment as well due to the component of centrifugal forces normal to the blade, which as well acts at the center of mass. In total, both the elastic flap and torsion response of the blade are well captured by the simulation in all cases with or without HHC. As in the case of the flap motion, there is virtually no difference in using the HHC wake geometry module or not due to the same reason as explained before.

Section Lift at 87% Radius

At a radial station of $r = 0.87$ (r = radial coordinate, made non-dimensional by the rotor radius) the model rotor was equipped with a chordwise pressure sensor instrumentation that allowed the integration of the pressure distribution to compute the section lift and moment. This radius as well is representative for the most important BVI locations responsible for noise radiation.

Therefore, the high frequency loading shows both the locations of BVI and its intensity. Here, the HHC wake geometry module will be very important. The presentation of results is split into two parts: firstly, the low frequency content (0-6/rev) of lift which is responsible for thrust and blade motion and secondly, the high frequency content (all above 6/rev) which contains all BVI events and is responsible for noise radiation. The low frequency content is compared to experimental data of HART II at the radial station $r = 0.87$ for the three fundamental cases as before in Fig. 8. In any case, the mean value as well as the low frequency content of the simulation (red) fits acceptably well to the experiment, and again the difference between inclusion of the HHC wake geometry module or computation without it is negligible, which could be assumed from the former results.

The HHC cases in general have the correct phase in the simulated results, just the magnitude is somewhat over-predicted, which is in agreement with the torsion

results for these cases, where the torsion amplitude as well is slightly larger than that in the experiment.

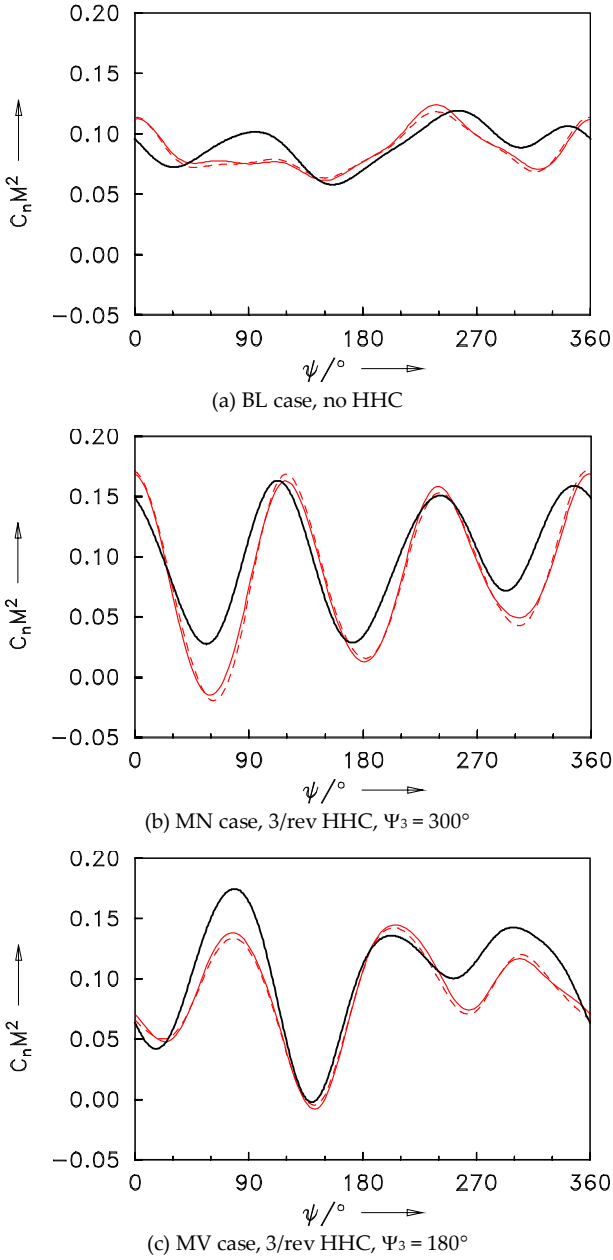


FIG. 8 SECTION LIFT AT 87% RADIUS, 0-6/REV

Vortex Induced Lift and BVI Locations

Due to its small size in terms of the core radius at the time of BVI in the range of 10-15% of the airfoil chord, any blade-vortex interaction is a high frequency event. The location where this event is going to happen is highly sensitive to the global operating condition, i.e. the orientation of the rotor disk relative to the flight direction, and the rotor thrust.

In addition, wake perturbations highly depend on the

harmonic rotor loading distribution [18]. To clarify the importance of the latter which is a main subject of this paper, as well as the demonstration even with prescribed wake codes, this can be addressed properly.

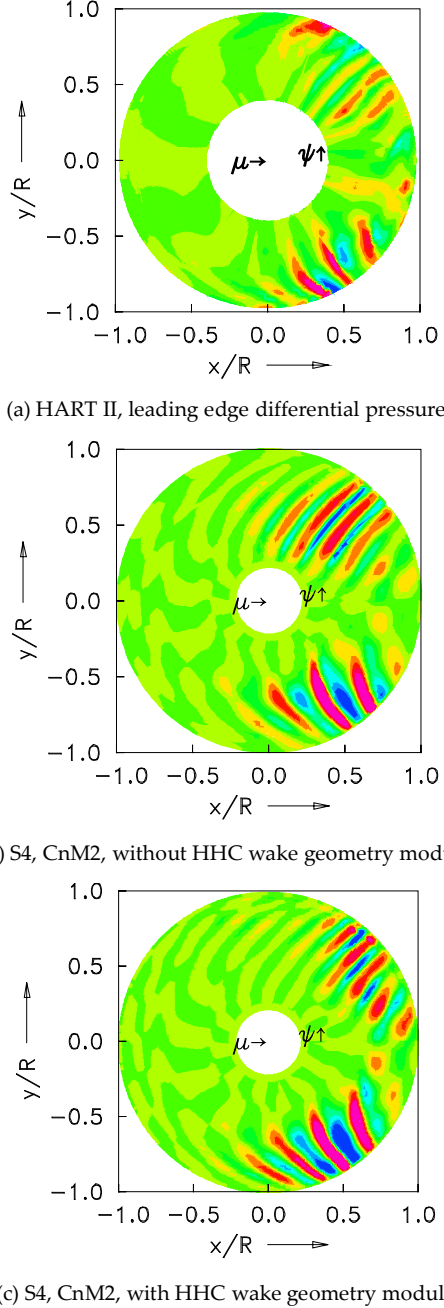


FIG. 9 BVI LOCATIONS AND INTENSITY, BL CASE, DATA > 6/REV

Firstly, this is shown at the example of the BL case without HHC in Fig. 9. Although being of less importance, this conventional operating condition already exhibits some dynamic fluctuations in the lift distribution seen in Fig. 8 (a), which will cause some – yet small – additional wake perturbations relative to classical prescribed wakes. Since the HART II experiment did not provide the section lift all along the span (just

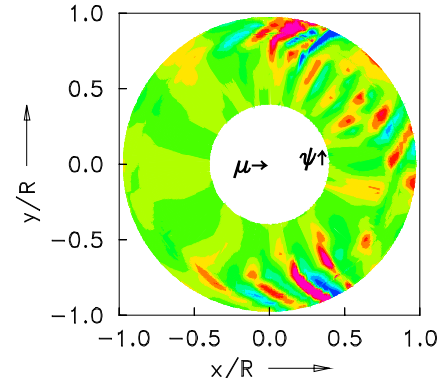
at 87% radius), for purposes of qualitative comparison, the leading edge differential pressure is compared here with the section loading of the simulation based on CnM2 airfoil coefficients and thus any information of blade pressure distributions can not be given. However, qualitatively both show BVI events in location and strength. This also is the reason why no scale is provided in Figs. 9, 10 and 11. In any case, the data are high-pass filtered such that all frequencies from 0-6/rev are removed.

Fig. 9 (b) shows results without and with usage of the HHC wake module (c). The general effect of the HHC wake geometry module is here that the BVI peak locations are radially shifted to little more outboard locations, otherwise the differences are small as expected and no general conclusion about the validity of the model can be drawn so far. Of more interest are the HHC cases with a large harmonic lift content and associated large additional wake deflections relative to the BL case.

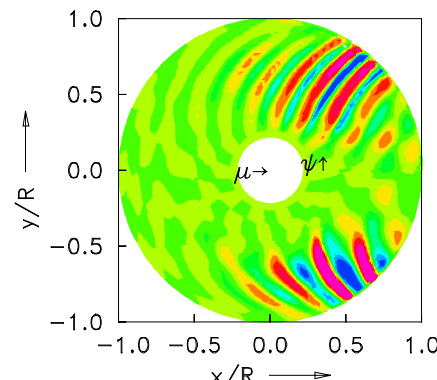
Results of the MN case are given in Fig. 10. Comparing the experimental data of the MN case in Fig. 10 (a) with that one of the BL case in Fig. 9 (a) two major effects can be extracted that are caused by HHC. Firstly, on the advancing side (1st quadrant), the BVI peak locations have moved significantly inboard and the passage of blade tip vortices through the rotor disk happening earlier in the MN case compared to the BL case. Since the interaction now happens more inboard where lower Mach numbers are present compared to those at the tip the noise radiation of these BVI will be less intensive. Secondly, the interaction locations on the retreating side (4th quadrant) have as well moved to the front of the disk and now are not any more parallel to the blade axis when the interaction takes place. This interaction geometry as well is a driving parameter of noise generation, which is maximum when parallel interactions happen like in the BL case.

In Fig. 10 (b) the S4 result using only classical prescribed wake is given. Compared to the BL case shown in Fig. 9 (b), the interaction locations have virtually not moved, and the only differences that show up are those due to different blade motion, which is virtually negligible since the vortex displacement due to HHC is one order of magnitude larger than the blade displacement. The inclusion of the HHC wake geometry module generates the result shown in Fig. 10 (c), which essentially has all features that the experiment in (a) has. On the advancing side, the trace of BVI has significantly moved inboard and on the retreating side,

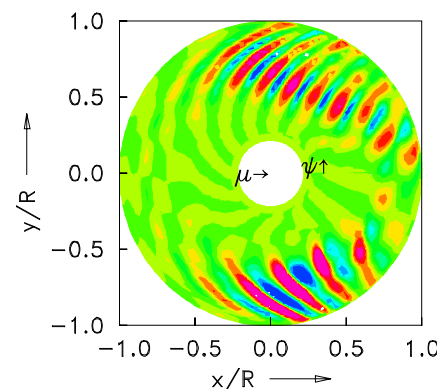
the BVI locations have moved forward within the rotor disk. On this qualitative basis the agreement with the experiment is very good.



(a) HART II, leading edge differential pressure



(b) S4, CnM2, without HHC wake geometry module



(c) S4, CnM2, with HHC wake geometry module

FIG. 10 BVI LOCATIONS AND INTENSITY, MN CASE, DATA > 6/REV

Finally, the MV case is investigated in the same manner. In Fig. 11 (a) the experimental data are given. They may be compared to both the BL case in Fig. 9 (a) and the MN case in Fig. 10 (a). Compared to the BL case, the azimuthal locations of BVI remain almost the same on both the advancing and retreating sides, but they have moved outboard towards the blade tip where the highest Mach numbers are present. Thus an increased noise radiation may be expected.

The classical prescribed wake generates a result shown in Fig. 11 (b). Compared to the result of the BL case in Fig. 9 (b) and the MN case in Fig. 10 (b) insignificant changes of the BVI locations are visible. As in the MN case, the only changes that can be seen are purely caused by a different blade motion. The inclusion of the HHC wake geometry module produces results as shown in Fig. 11 (c). As in the experimental data, there is a clear movement of the BVI locations towards the blade tip, especially on the advancing side, where the majority of noise is generated due to the larger Mach numbers compared to those present on the retreating side.

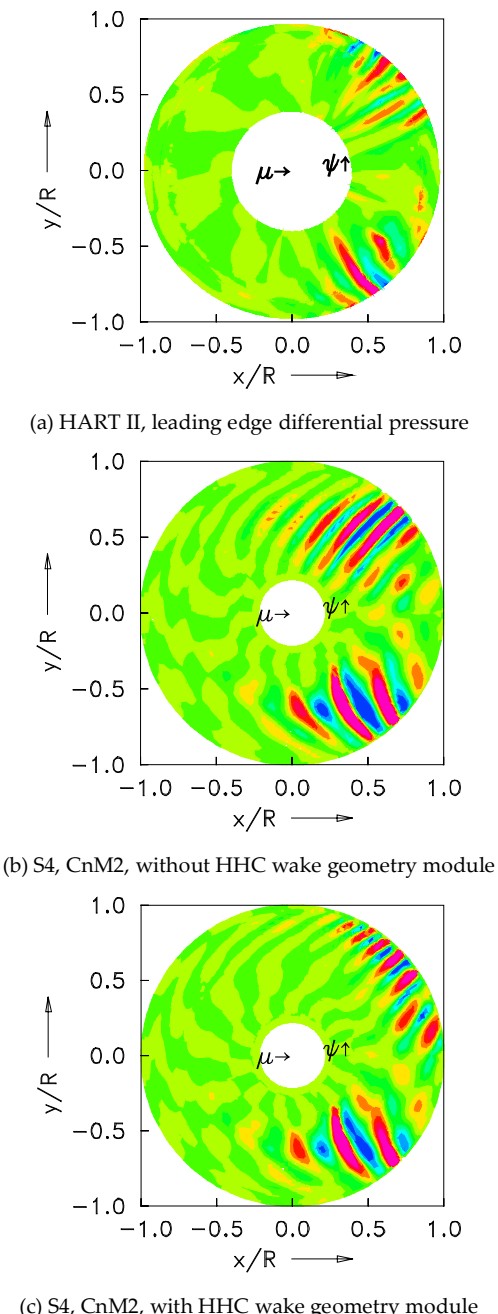


FIG. 11 BVI LOCATIONS AND INTENSITY, MV CASE,
DATA > 6/REV

From these results – at least from a qualitative point of view – the HHC wake geometry module produces the changes of BVI locations relative to the BL case without HHC in a correct trend. However, although this is a promising first result, it does only focus on the events within the rotor disk and fails to tell how good it is with respect to the entire tip vortex trajectory, i.e. the tip vortex flight path from its point of creation through the rotor disk with all the vertical up- and downwards convection.

The same interaction location can be obtained with very different vortex trajectories – one flying very flat over the disk and another one flying initially pretty far upwards away from the disk, then turning to a steep downwards trajectory. The interaction location with a rotor blade may in both cases be the same.

Tip Vortex Trajectories

Next, the tip vortex trajectories of the HART II data are compared to the prescribed wake results for two lateral positions: $y/R = \pm 0.7$ (+: advancing side; -: retreating side). First of all, the corrected Beddoes' wake geometry is used with the longitudinal gradient of the induced inflow of k_x from Table 1 (denoted as "classic wake" in the following figures). Secondly, the modified gradient is used (i.e., $1.7 \cdot k_x$) together with the HHC wake geometry module. The latter does not play a major role in the BL case as shown before.

Results of the BL case are given in Fig. 12 (a) for the advancing side and in (b) for the retreating side. It can clearly be seen that the classic formulation has a much flatter trajectory than the experimental data, which has been already shown in Fig. 2 and in Fig. 4. The reason is that the longitudinal gradient of induced inflow, k_x , is too small. The improvements that can be obtained using the modified value of k_x are clearly visible: now the prescribed wake geometry is much closer to the experimental data. On the retreating side there is an almost perfect match with the trajectory as measured during HART II.

Next, the same lateral position is taken to compare vortex trajectories in the two HHC cases. Here the HHC wake geometry module must show the additional wake deflections due to active control of the rotor. For the MN case this is shown in Fig. 13, again in (a) for the advancing and in (b) for the retreating side. Of special interest and importance is the relative change of the trajectory with respect to the BL case, since the only difference is the addition of the HHC control, which modifies slightly the blade position but

largely the wake geometry, i.e. the tip vortex trajectories.

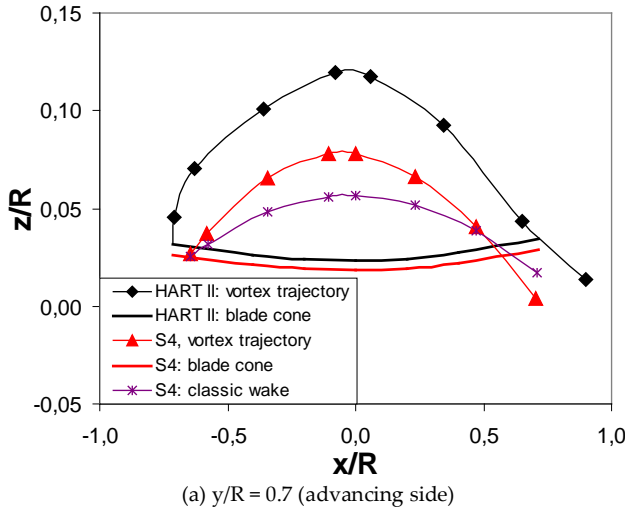
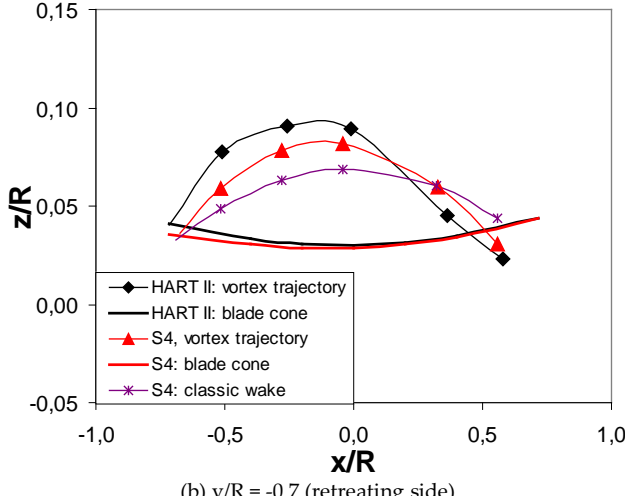
(a) $y/R = 0.7$ (advancing side)(b) $y/R = -0.7$ (retreating side)

FIG. 12 TIP VORTEX TRAJECTORIES, BL CASE

Based on the comparison between Fig. 13 (a) with Fig. 12 (a), the experimental data clearly show a much stronger downwards convection of the tip vortex in the MN case. Since the classical prescribed wake formulation does not account for any harmonic loading due to HHC or other reasons, the tip vortex trajectory is virtually the same in both the BL and MN cases. This is significantly changed when using the HHC wake geometry module. Here, the same trend as observed in the experiment is generated that the tip vortex trajectory is strongly convected downwards due to the HHC-related loading. This loading is increased relative to the BL case – see Fig. 8 (a) and (b) – at an azimuth of 135° , which is at the left side of Fig. 13, and consequently the induced downwash is proportionally increased, which is responsible for the stronger downwards vortex convection.

A similar observation can be made on the retreating

side, Fig. 13 (b), which must be compared to the appropriate part of the BL case, i.e. Fig. 12 (b).

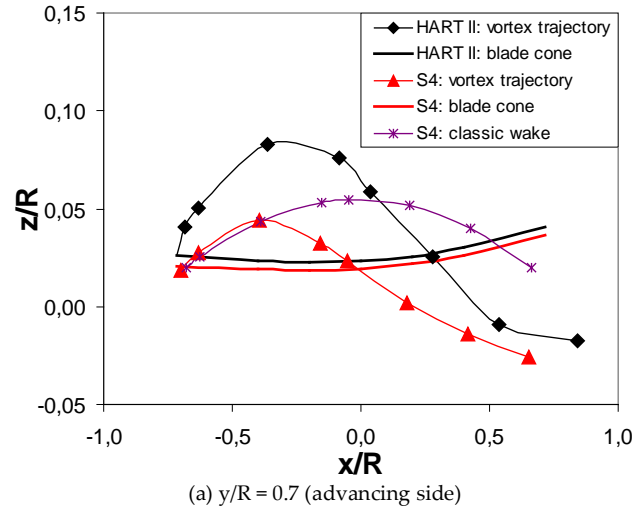
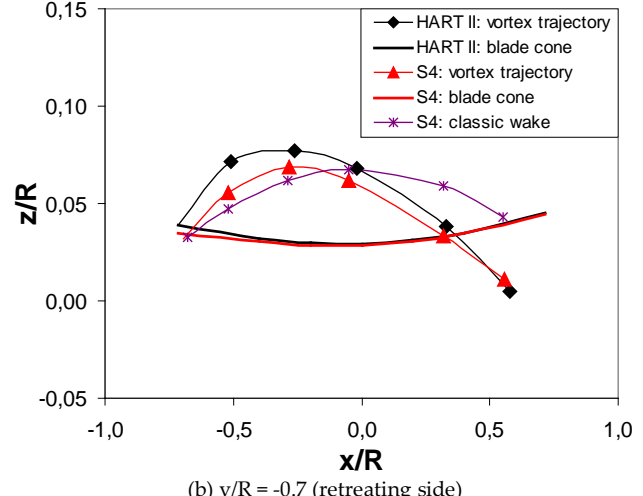
(a) $y/R = 0.7$ (advancing side)(b) $y/R = -0.7$ (retreating side)

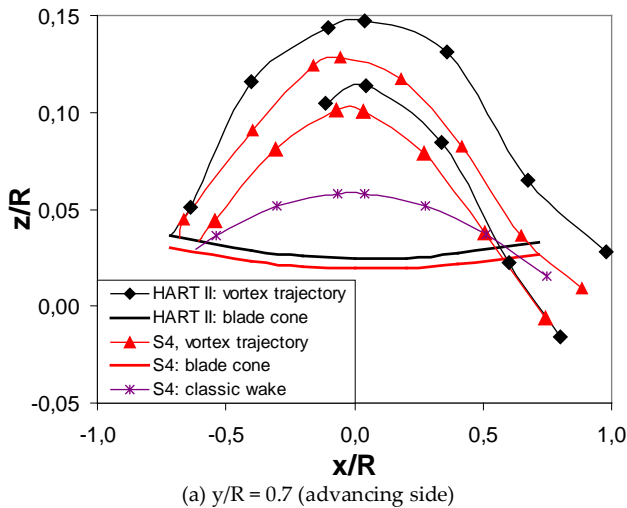
FIG. 13 TIP VORTEX TRAJECTORIES, MN CASE

Although not as strong as on the advancing side there is slightly more lift to the left of the figure due to HHC, and thus a slightly increased downwash. The vortex trajectory in the MN case is thus a little lower than that in the BL case, and again this is correctly predicted by the HHC wake geometry module.

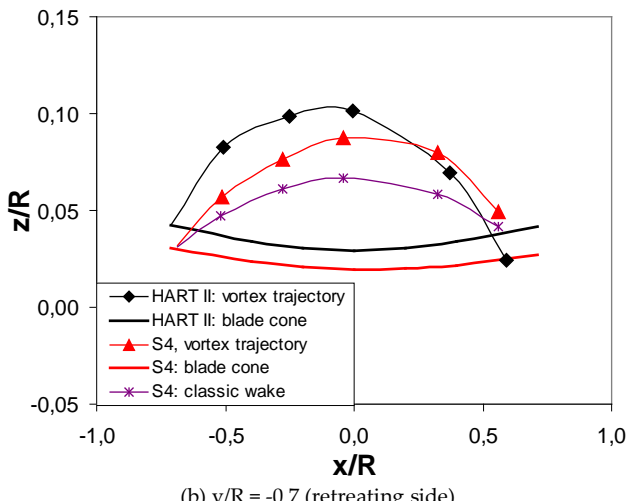
The last comparison is made with the same location in the MV case, which has the same HHC blade pitch control amplitude, but a different control phase. Therefore, the areas in the rotor disk where additional lift or download is generated by HHC are shifted to different azimuth positions. On the advancing side even a local download is present at the blade tip at $y/R = 0.7$. The vortex generated at the blade tip therefore rotates in opposite direction, compared to the BL and MN cases (both of them exhibit lift on the blade tip, see Fig. 8 (a) and (b), while the MV case in Fig. 8 (c) shows negative lift = download at 135° azimuth, which

is about $y/R = 0.7$.

More inboard of the blade, the download turns into lift again, and this radial change of blade circulation causes a secondary vortex to be generated at an inboard location [16], [18], which roughly is located at 80% radius.



(a) $y/R = 0.7$ (advancing side)



(b) $y/R = -0.7$ (retreating side)

FIG. 14 TIP VORTEX TRAJECTORIES, MV CASE

Due to this download, an induced upwash is generated that convects the tip vortex further up compared to that in the BL case. This is clearly seen in Fig. 14 (a), which must be compared to the same location of the BL case in Fig. 12 (a) and to the MN case in Fig. 13 (a). The tip vortex now is moved far atop the rotor disk and does not even pass it any more at the right side of the figure. Also, a secondary vortex could be measured with opposite sense of rotation than that of the tip vortex as explained before. This secondary vortex is formed by a roll-up procedure of strong but radially distributed vorticity that is trailed into the wake behind the blade from a strong radial gradient of blade circulation.

During this roll-up, it is very difficult to identify a vortex center in the velocity measurement data, which is the reason why the experimental data do not start at the blade. The HHC wake geometry module, however, allows for tracing back the inboard vortex up to the point of creation. The general trend of trajectory prediction appears to nicely match the experimental data. The conventional prescribed wake formulation, however, again does not react to such loading and inflow modifications and thus its trajectory is virtually unchanged relative to the BL and MN cases. The retreating side is given in Fig. 14 (b), which must be compared to the BL case in Fig. 12 (b) and the MN case in Fig. 13 (b). To the left of the figure the MV case has a less lift than the MN case, thus less downwash is created and the vortex trajectory is consequently more upwards. Like in the MN case, this trend is predicted by the HHC wake geometry module.

BVI Noise Radiation

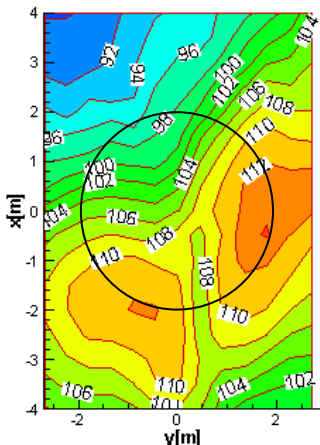
The final goal of any such high fidelity rotor simulation is to compute the mid-frequency BVI noise radiation sufficiently well, and especially the changes of noise intensity due to changes in rotor operating condition, which in this case is the application of HHC. In the following figures, the BVI sound pressure levels based on 6-40 blade passage frequency are given in dB. The HART II data represent the average spectra of 100 individual measurements.

Firstly, the BL case is investigated and results of the HART II test, the simulation with conventional prescribed wake and the simulation with the inclusion of the HHC wake geometry module are shown in Fig. 15 (a), (b) and (c). It can be seen that the conventional wake approach works quite well in this case, although on the advancing and retreating side the intensity is missed, which is also the case in the wake geometry including the enhancements. The drop of HART II noise levels in the centerline $y/R = 0$ from the rotor center towards the rear of the disk is due to the fuselage fairing which is not taken into account in the simulated noise radiation.

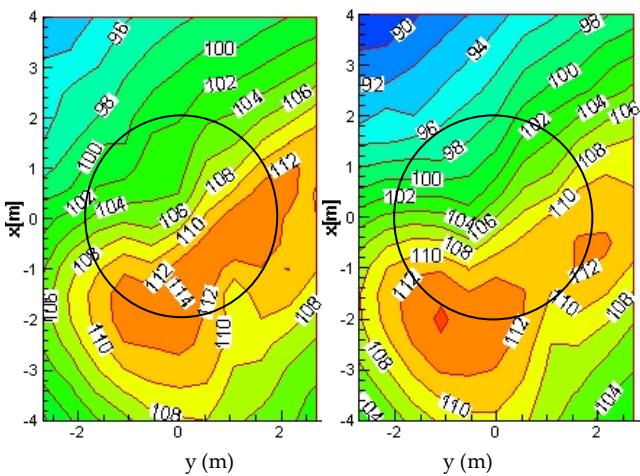
The ultimate test of the model, however, is in the application to HHC conditions. The conventional prescribed wake approach does not respond in the wake geometry to any dynamic load distributions in the rotor disk and the only changes in wake geometry are due to changes in blade motion. Nevertheless, all changes of aerodynamic loading alter the vortex circulation strength, which is included in both the conven-

tional approach and in the model with the HHC wake geometry module. The latter also tries to represent the additional wake geometry modifications due to any harmonic load distribution.

Results are next shown for the MN and for the MV case, where 3/rev HHC is applied. The MN case should exhibit less noise than the BL case, and even more important, a change of directivity. This is seen when comparing the experimental data for MN in Fig. 16 (a) with one of the BL case in Fig. 15 (a). The conventional wake generates significantly more noise (Fig. 16 (b) compared with the BL results in Fig. 15 (b)). This is due to virtually unchanged BVI locations and in addition the strength of the interacting tip vortex is stronger than that in the BL case – see the loading in Fig. 8 (a)-(b). This has been already observed in the high frequency load distribution part shown in Fig. 9-11 and in the vortex trajectories shown in Fig. 12-14.



(a) HART II test (wind direction from top to bottom)

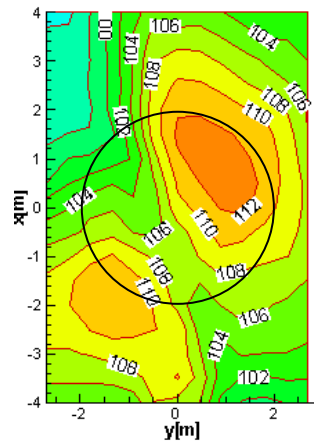


(b) S4 with classic wake (c) S4 with HHC wake geometry module

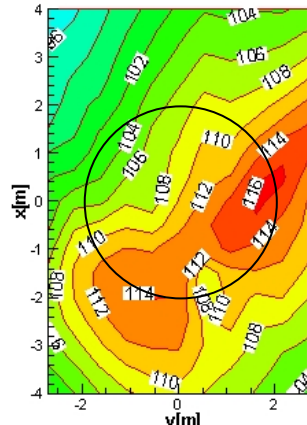
FIG. 15 MID-FREQUENCY BVI NOISE RADIATION, BL CASE

The results with the HHC wake geometry module are given in Fig. 16 (c). Compared to the BL case in Fig. 15

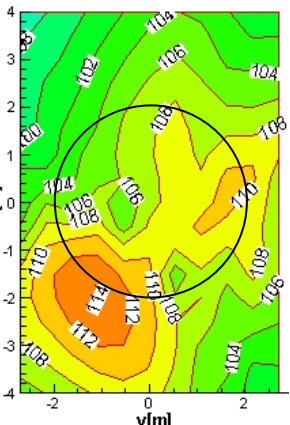
(c) a noise level reduction is predicted, although more than measured in the experimental data. Moreover, the tendency towards a directivity change more to the front of the disk is indicated by the result. However, it appears that the job is somewhat “overdone”, i.e. the wake deflections appear larger than they should be with the consequences on the results as mentioned. The last validation is made with the MV case. Here a different HHC control phase is applied and thus the harmonic air load distribution is rotated in the rotor disk by the difference of the control phases. In terms of rotor azimuth, this is $\Delta\Psi = \Delta\Psi_3/3 = (300^\circ - 180^\circ)/3 = 40^\circ$.



(a) HART II test (wind direction from top to bottom)



(b) S4 with classic wake



(c) S4 with HHC wake geometry module

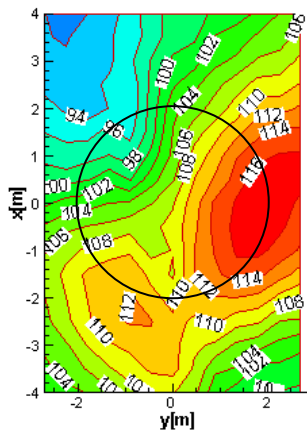
FIG. 16 MID-FREQUENCY BVI NOISE RADIATION, MN CASE

Results for MV are shown in Fig. 17. The conventional wake geometry has not changed, thus its directivity is the same as before and the different noise intensity is only due to different vortex circulation strengths. The inclusion of the HHC wake geometry module in Fig. 17 (c) has also higher levels than the BL case, yet lower than the experiment. In addition, the reason appears to be in “overdoing” the wake modifications. As seen in the high frequency blade air loads in Fig. 11 (c) the BVI locations have moved into the right direction, but

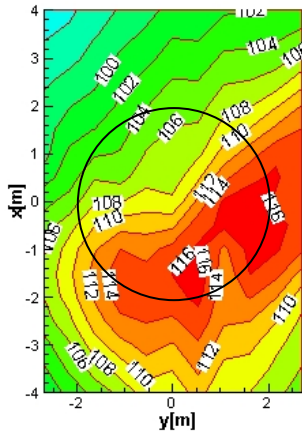
more than in the experiment. Several interactions are now outside the disk instead of at the blade tip area. It is assumed that this is partly due to the modification of the inflow gradient, which was set at twice the value of Beddoes, see Fig. 3.

Verification of the Inflow Gradient

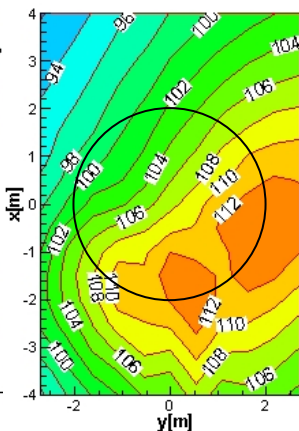
At the beginning of this paper, the longitudinal gradient of the underlying global induced inflow model was more or less arbitrarily set to $1.7 \cdot k_x = 2.633$. The proof was only made via a better agreement with the measured vortex trajectory in Fig. 2 and Fig. 4.



(a) HART II test (wind direction from top to bottom)



(b) S4 with classic wake



(c) S4 with HHC wake geometry module

FIG. 17 MID-FREQUENCY BVI NOISE RADIATION, MV CASE

The question remains whether the actual resulting wake and its induced inflow velocity field indeed approach this higher value. For this purpose the induced velocity field that is only computed at the blade elements is taken and at a longitudinal cut at the lateral position of interest, i.e. $y/R = 0.7$, these data are extracted from the simulation.

The result is shown in Fig. 18. At the right side a strong BVI is visible. Although the distribution of data is highly non-linear in general due to all the discrete

vortices and their circumferential flow field, the global trend is clearly linearly increasing from left to right. The negative values to the left indicate upwash at the front of the rotor disk, which is caused by the first tip vortex downstream of this location.

Thereafter the induced inflow is essentially linearly increasing as suggested by many authors. However, the linear gradient that can be extracted by means of regression analysis has a value of $k_x = 2.4$ on the advancing and $k_x = 2.6$ on the retreating side, which is significantly larger than most of the values suggested by various authors and listed in Table 1, but quite close to the value of $k_x = 2.633$ as used in this study.

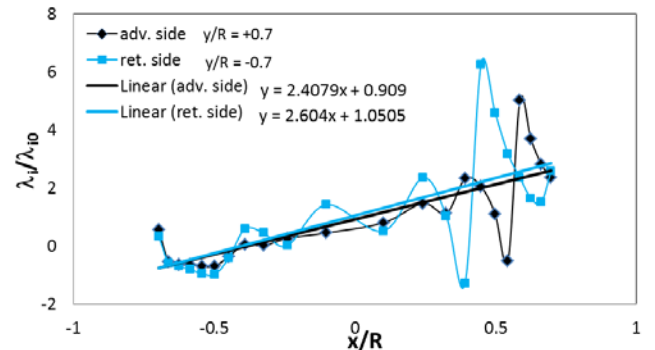


FIG. 18 INDUCED INFLOW OF THE MODIFIED WAKE

The value of k_x should be modified according to the results obtained within the wake simulation itself in order to represent an overall consistent approach. In future, an automatic iterative procedure is foreseen that analyses this gradient at every wake iteration and applies it to the next geometry computation. The lateral gradient can be dealt with in the same manner.

Conclusions

Conventional prescribed wake codes cannot simulate the effects of higher harmonic air loads distribution (like those caused by active rotor control) on the wake geometry with respect to BVI locations and their intensity, thus they must fail to predict the noise radiation. This applies to both, active control situations and high speed flight conditions where increasingly larger higher harmonic loading is also generated by the aerodynamic environment.

It is possible to account for wake deflections caused by the harmonic blade loading distribution – at least to a first order of accuracy – originating from active control, HHC, or flight condition. These are added to the geometry of any conventional prescribed wake geometry.

The combination of elastic blades, unsteady lifting line aerodynamics and prescribed wake including deflec-

tions due to the higher harmonic air load distribution within the rotor disk leads to a significant improvement in prediction of noise radiation for both the baseline condition without and with HHC, here it is demonstrated at the example of 3/rev HHC.

Prescribed wake codes are able to predict BVI noise radiation correctly in trend, and also the changes of noise radiation with respect to HHC or other sources of higher harmonic air loads. The pre-requisite is that a model is applied which accounts for additional wake deflections due to rotor harmonic loading.

The HHC wake geometry module accounts for flight speed and thus it is considered generic.

ACKNOWLEDGMENT

The HART II data are the result of international cooperation involving US Army AFDD, NASA Langley, DNW, ONERA and DLR. The authors highly appreciate the contributions of each partner in this program.

REFERENCES

Beddoes, T.S. "A Wake Model for High Resolution Air loads." International Conference on Rotorcraft Basic Research, Research Triangle Park, NC, USA, 1985.

Brentner, K.S., Farassat, F. "An Analytical Comparison of the Acoustic Analogy and Kirchhoff Formulation for Moving Surfaces." *AIAA Journal* 36 (8), 1998: 1379-1386.

Burley, C.L., Brooks, T.F., van der Wall, B.G., Richard, H., Raffel, M., Beaumier, P., Delrieux, Y., Lim, J.W., Yu, Y.H., Tung, C., Pengel, K., Mercker, E. "Rotor Wake Vortex Definition Using 3C-PIV Measurements - Corrected for Vortex Orientation." *AIAA Paper 2003-3175*, 9th AIAA/CEAS Aeroacoustics Conference, Hilton Head, South Carolina, USA, 2003.

Dietz, M., Krämer, E., Wagner, S. "Tip Vortex Conservation on a Main Rotor in Slow Descent Flight using Vortex-adapted Chimera Grids." 24th AIAA Applied Aerodynamics Conference, Paper AIAA-2006-3478, San Francisco, CA, USA, 2006.

Ffowcs Williams, J.E., Hawking, D.L. "Sound Generation by Turbulence and Surfaces in Arbitrary Motion." *Philosophical Transactions of the Royal Society*, A264, 1969: 321-342.

Hashimoto, A., Nakamura, Y., Saito, S., Aoyama, T., Yang, C. "Aeroelastic Simulation of HART II Model Using Moving Overlapped Grid Approach." 32nd European Rotorcraft Forum, Maastricht, Netherlands, 2006.

Kelly, M.E., Duraisamy, K., Brown, R.E. "Predicting Blade Vortex Interaction, Airloads and Acoustics using the Vorticity Transport Model." American Helicopter Society Specialists' Conference on Aeromechanics, San Francisco, CA, USA, 2008.

Küssner, H.G. "Zusammenfassender Bericht über den instationären Auftrieb von Flügeln." *Luftfahrtforschung* 13 (12), 1936: 410-424.

Leishman, J.G., Principles of Helicopter Aerodynamics, Cambridge University Press, 2000.

Leiss, U. "A Consistent Mathematical Model to Simulate Steady and Unsteady Rotor-Blade Aerodynamics." 10th European Rotorcraft Forum, The Hague, Netherlands, 1984.

Lim, J.W. "An Assessment of Rotor Dynamics Correlation for Descending Flight Using CFD/CSD Coupled Analysis." 64th Annual Forum of the American Helicopter Society, Montreal, Canada, 2008.

Lim, J.W., Nygaard, T.A., Strawn, R., Potsdam, M. "Blade-Vortex Interaction Airloads Prediction Using Coupled Computational Fluid and Structural Dynamics." *Journal of the American Helicopter Society* 52 (4), 2007: 318-328.

Mangler, K.W., Squire, H.B. "The Induced Velocity Field of a Rotor." *ARC Reports & Memoranda* 2642, 1950.

Perez, G., Bailly, J., Rahier, G. "Using the HART II Database to Improve BVI Noise Prediction." *Journal of the American Helicopter Society* 53 (1), 2008: 56-67.

Schneider, O. "Analysis of SPR Measurements of HART II." *Aerospace Science and Technology* 9 (5), 2005: 409-420.

The HART II International Workshop Data Base: <ftp://HART-II@ftp.dlr.de>; password: HART-II.

Theodorsen, T. "General Theory of Aerodynamic Instability and the Mechanism of Flutter." *NACA Rep. 496*, 1935.

van der Wall, B.G., Burley, C.L., Yu, Y.H., Pengel, K., Beaumier, P. "The HART II Test - Measurement of Helicopter Rotor Wakes." *Aerospace Science and Technology* 8 (4), 2004: 273-284.

van der Wall, B.G., Richard, H. "Analysis Methodology for 3C PIV Data of Rotary Wing Vortices." *Experiments in Fluids* 40 (5), 2006: 798-812.

van der Wall, B.G., Yin, J. "DLR's S4 Rotor Code Validation

with HART II Data: The Baseline Case." International Forum on Rotorcraft Multidisciplinary Technology, Seoul, Korea, 2007.

van der Wall, B.G. "The effect of HHC on the Vortex Convection in the Wake of a Helicopter Rotor." *Aerospace Science and Technology* 4 (5), 2000: 320-336.

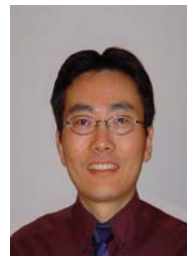
van der Wall, B.G. "Analytic Formulation of Unsteady Profile Aerodynamics and its Application to Simulation of Rotors." *ESA-TT-1244*, 1992.

Yin, J., Delfs, J. "Improvement of DLR Rotor Aeroacoustic Code (APSIM) and its Validation with Analytic Solution." 29th European Rotorcraft Forum, Friedrichshafen, Germany, 2003.



B.G. van der Wall was born in Oldenburg (Germany) in 1958. He received his Diploma degree in Aeronautical Engineering from TU Braunschweig (Germany) in 1986; a Master's degree in Aerospace Engineering from University of Maryland (USA) in 1991; a Doctoral degree from TU Braunschweig in 1999;

and became Senior scientist of DLR in 2011. Since 1986 he has been working at the German Aerospace Center (DLR) in the Helicopter Branch of the Institute of Flight Systems in Braunschweig. His main work was devoted to development of a high resolution rotor code including flexible blades, unsteady aerodynamics and vortex wake as basic tool for evaluation of any kind of active rotor control technology. Experiments with rotors in the large low-speed wind tunnel of DNW were performed partly under his guidance, especially the HART II test, which was awarded in 2004 with the Howard Hughes Award and in 2012 with the AgustaWestland International Fellowship Award for the HART II International Workshop which was initiated and headed by him. He has published 90 papers in Journals and conferences.



Jianping Yin has been working as a Research Engineer at the Helicopter Branch at DLR's Institute of Aerodynamics and Flow Technology since 1998. He obtained his doctorate from Nanjing University Aerodynamics Department in Nanjing, China. His main work was devoted to development of aeroacoustic tools for analyzing helicopter noise generation, propagation and reduction mechanism. Currently, he is the DLR responsible for the ONERA/ DLR research field on quiet and comfortable rotorcraft.